Debonding Failure and Volume Fraction Effects in Micro-reinforced Composites of AA2024/Silicon Oxide

[1]H. B. Nirnajan and A. Chennakesava Reddy

[1]Assoicate Professor, Department of Mechanical Engineering, M. S. R. I.T, Bangalore, India
[2]Assistant Professor, Department of Mechanical Engineering, MJ College of Engineering and Technology, Hyderabad, India
dr_acreddy@yahoo.com

Abstract: A square array unit cell/2-D diamond particulate RVE models were employed to understand interfacial debonding using cohesive zone analysis. The particulate metal matrix composites are silicon oxide/AA2024 alloy at different volume fractions of silicon oxide. Interface debonding was observed in all the composites. The maximum stress concentration occurs at the particulate–matrix interface along the loading direction.

Keywords: AA2024, silicon oxide, diamond particulate, RVE model, finite element analysis, interface debonding.

1. INTRODUCTION

Effective transport properties of a composite can be significantly affected by the presence of imperfect interfaces between its constituents, as shown experimentally by Garret and Rosenberg [1] and Hasselman and Donaldson [2]. The micro-scale interfacial effects in particulate-reinforced composites are studied using generalized plane strain by means of the finite element analysis [2-16].

In the present research, assuming a periodic distribution of particulate in the matrix (figure 1), a unit cell is chosen including two quarter-diamond particulates. The interfacial debonding analysis was carried out using cohesive zone models in AA2024/silicon oxide nanoparticulate-reinforced metal matrix composites.

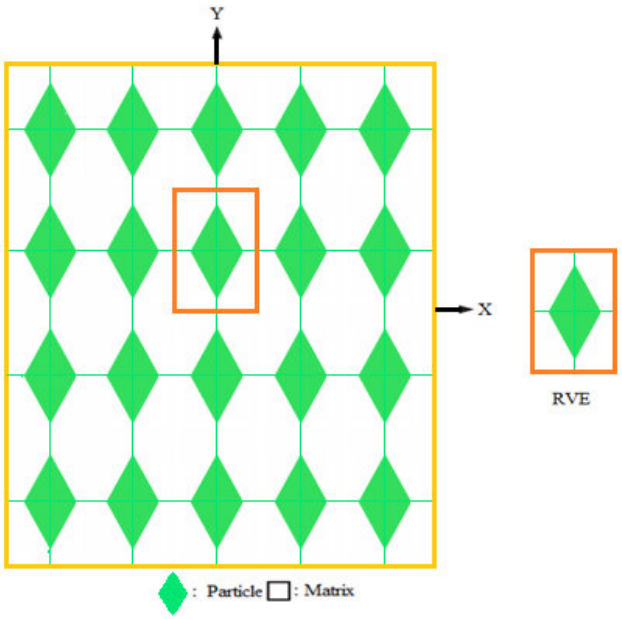

Figure 1: The RVE model.

2. MATERIALS AND METHODS

The volume fractions of silicon oxide used in the present work were 10%, 20%, and 30%. The matrix material was AA2024 alloy. The periodic model for the representative volume element (RVE) scheme was constructed from 2-D diamond

particulates in a square array particulate distribution (figure 1). PLANE183 element was used for the matrix and the nanoparticulates. The cohesive zone can be incorporated in the continuum formulation by applying the cohesive tractions as boundary conditions. The cohesive element is implemented as a linear element with four nodes. The iso-parametric formulation is chosen for the element, meaning that shape and displacements are interpolated by the same shape functions.

Shear-log model is based on the assumption that all of the load transfer from matrix to particulate occurs via shear stresses acting on the particulate interface between the two constituents. The rate of change of the stress in the particulate to the interfacial shear stress at that point and the particulate radius, 'r' is given by:

$$\frac{d\sigma_p}{dx} = -\frac{2\tau_i}{r} \quad (1)$$

which may be regarded as the basic shear lag relationship.

The stress distribution in the particulate is determined by relating shear strains in the matrix around the particulate to the macroscopic strain of the composite. Some mathematical manipulation leads to a solution for the distribution of stress at a distance 'x' from the mid-point of the particulate which involves hyperbolic trig functions:

$$\sigma_p = E_p\varepsilon_c[1 - cosh(nx/r)sech(ns)] \quad (2)$$

where ε_c is the composite strain, s is the particulate aspect ratio (length/diameter) and n is a dimensionless constant given by:

$$n = \left[\frac{2E_m}{E_p(1+v_m)ln(1+v_p)}\right]^{1/2} \quad (3)$$

in which v_m is the Poisson ratio of the matrix. The variation of interfacial shear stress along the particulate length is derived, according to Equation (1), by differentiating this equation, to give:

$$\tau_i = \frac{n\varepsilon_c}{2}E_p sinh\left(\frac{nx}{r}\right)sech(ns) \quad (4)$$

The equation for the stress in the particulate, together with the assumption of a average tensile strain in the matrix equal to that imposed on the composite, can be used to evaluate the composite stiffness. This leads to:

$$\sigma_c = \varepsilon_c\left[v_pE_p\left(1 - \frac{tanh(ns)}{ns}\right) + (1 - v_p)E_m\right] \quad (5)$$

The expression in square brackets is the composite stiffness. The stiffness is a function of particulate aspect ratio, particulate/matrix stiffness ratio and particulate volume fraction.

If the particle deforms in an elastic manner (according to Hooke's law) then,

$$\tau = \frac{n}{2}\sigma_p \quad (6)$$

If particle fracture occurs when the stress in the particulate reaches its ultimate tensile strength, $\sigma_{p,uts}$, then setting the boundary condition at

$$\sigma_p = \sigma_{p,\,uts} \quad (7)$$

and substituting into Equation (6) gives a relationship between the strength of the particle and the interfacial shear stress such that if

$$\sigma_{P,uts} < \frac{2\tau}{n} \quad (8)$$

Then the particle will fracture. Similarly if interfacial debonding/yielding is considered to occur when the interfacial shear stress reaches its shear strength

$$\tau = \tau_{max} \quad (9)$$

For particle/matrix interfacial fracture can be established whereby,

$$\tau_{max} < \frac{n\sigma_p}{2} \quad (10)$$

This approach suggests that the outcome of a matrix crack impinging on an embedded particle depends on the balance between the particle strength and the shear strength of the interface.

For plane strain conditions, the macro stress- macro strain relation is as follows:

$$\begin{Bmatrix}\overline{\sigma_x}\\ \overline{\sigma_y}\\ \overline{\tau_{xy}}\end{Bmatrix} = \begin{bmatrix}\overline{C_{11}} & \overline{C_{12}} & 0\\ \overline{C_{21}} & \overline{C_{22}} & 0\\ 0 & 0 & \overline{C_{33}}\end{bmatrix} \times \begin{Bmatrix}\overline{\varepsilon_x}\\ \overline{\varepsilon_y}\\ \overline{\gamma_{xy}}\end{Bmatrix} \quad (11)$$

The interfacial tractions can be obtained by transforming the micro stresses at the interface as given in Eq. (3):

$$t = \begin{Bmatrix}t_z\\ t_n\\ t_t\end{Bmatrix} = T\sigma \quad (12)$$

where, $T = \begin{bmatrix} 0 & 0 & 0 \\ cos^2\theta & sin^2\theta & 2sin\theta cos\theta \\ -sin\theta cos\theta & sin\theta cos\theta & cos^2\theta - sin^2\theta \end{bmatrix}$

3. RESULTS AND DISCUSSION

The tensile modulus increased with volume fraction of silicon oxide while compression modulus decreased as shown figure 2a. The shear modulus was unchanged with increase in the volume fraction of SiO_2 in the composites (figure 2b). The major Poisson's ratios decreased with volume fraction of silicon oxide (figure 2c). The difference in the elastic moduli of SiO_2 particulates and AA2024 alloy matrix is marginal of 0.7 GPa. The Poisson's ratios of AA2024 alloy matrix and SiO_2 particulates are, respectively, 0.33 and 0.17. Since Young's modulus of particulate in the longitudinal direction is much greater than that of the matrix, particulate dominates the longitudinal stiffness of the composite.

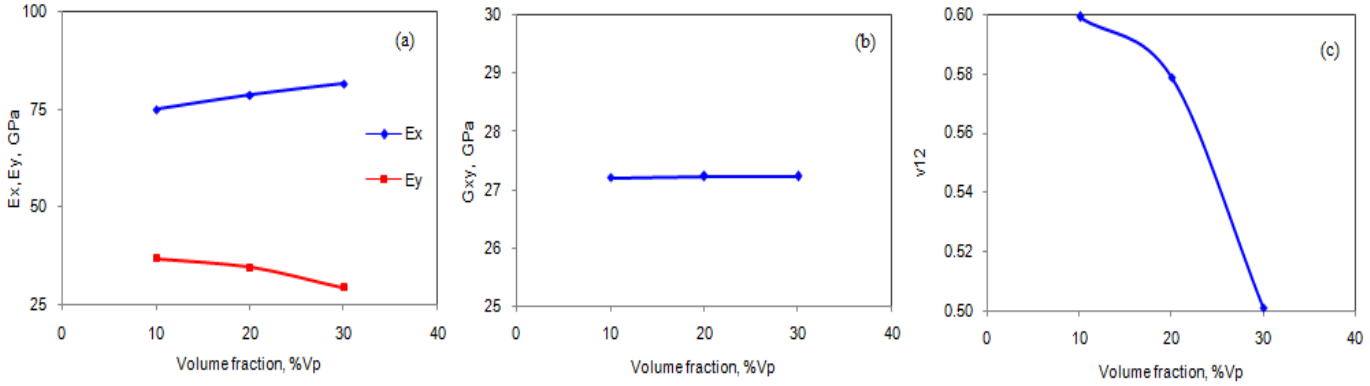

Figure 2: Effect of volume fraction on effective material properties.

The condition $\tau_{max} < n\sigma_p/2$ satisfied for the occurrence of debonding in the composites including 10%, 20% and 30% SiO_2 (figure 3a). The SiO_2 particulate fracture was not found in the AA2024/SiO_2 composites as shown in figure 3b as the condition $\sigma_p \leq 2\tau/n$ did not satisfied.

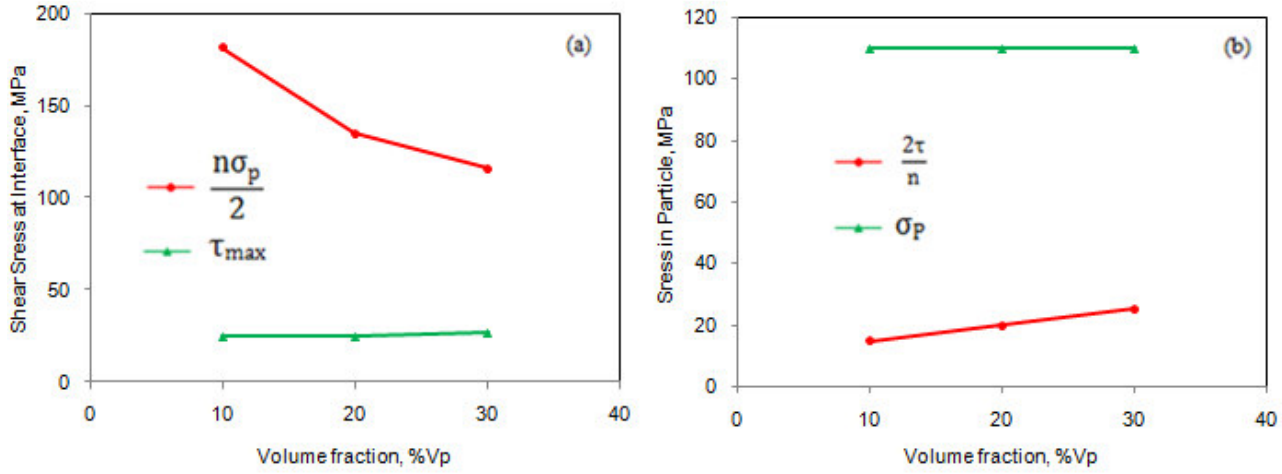

Figure 3: Fracture criteria of: (a) interface debonding and (b) particulate fracture.

The strain energy density increased at the interface with an increase in the volume fraction of SiO_2 (figure 4). The normal and tangential tractions are plotted in figure 5. Because of symmetry considerations, the variations of the interface stresses with circumferential location are plotted only for the range $0^o \leq \theta \leq 90^o$. For AA2024/30%$SiO_2$ composites, the normal tractions are higher than that for AA2024/10%SiO_2 and AA2024/20%SiO_2 composites. The interface debonding occurred between $0^o \leq \theta \leq 70^o$. In this work, the fibers behave purely elastic while the matrix is considered as isotropic with an either purely elastic or elasto-plastic behavior. This extended unit cell study of composites focuses on the progressive particulate-matrix debonding when one particulate experiences a neighboring particulate with a dissimilar interfacial strength.

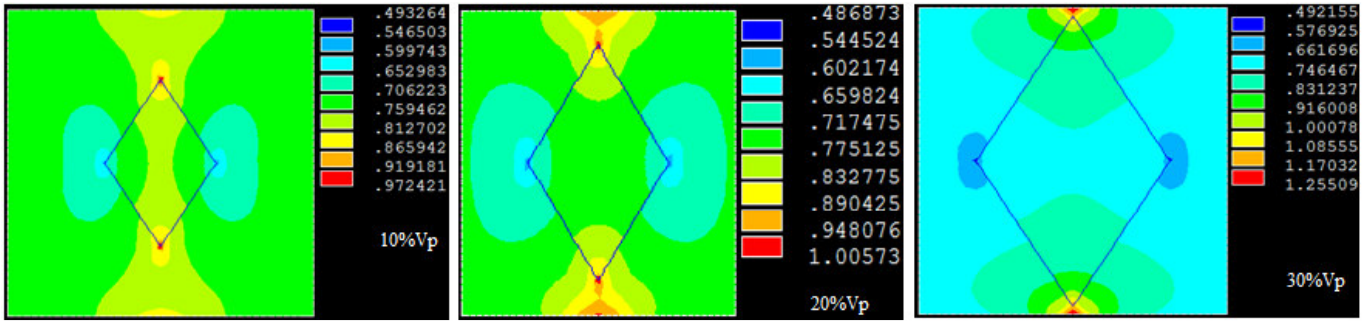

Figure 4: Strain energy densities of cohesive zones obtained from finite element analysis for debonding.

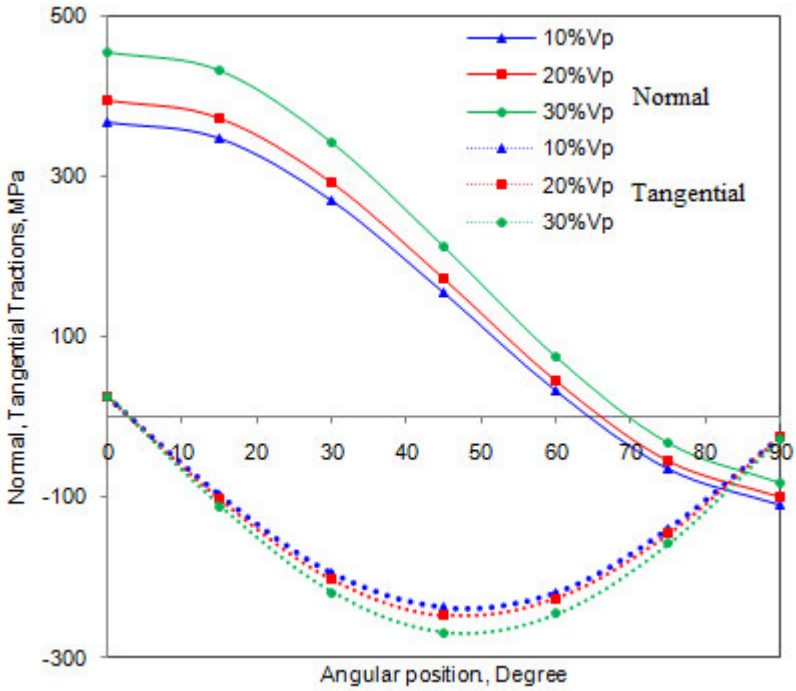

Figure 5: Normal and tangential: (a) tractions and (b) displacements.

4. CONCLUSION

The interface debonding occurred in the composites containing 10%, 20% and 30% volume fractions SiO_2. The maximum stress concentration occurs at the particulate–matrix interface along the loading direction, whereas minimum stress concentration occurs in the matrix near the interface along the y-direction, which is perpendicular to the loading direction.

REFERENCES

1. Garret KW, Rosenberg HM (1974) The thermal conductivity of epoxy-resin powder composite materials, Materials. J. Phys. D 7:1247-1258.
2. Hasselman DPH, Donaldson KY (1992) Effect of reinforcement particle size on the thermal conductivity of a particulate-silicon carbide-reinforced aluminum matrix composite, J. Am. Ceram. Soc. 75:3137-3140.
3. A. Chennakesava Reddy, Assessment of Debonding and Particulate Fracture Occurrences in Circular Silicon Nitride Particulate/AA5050 Alloy Metal Matrix Composites , National Conference on Materials and Manufacturing Processes, Hyderabad, India, 27-28 February1998, pp.104-109.
4. B. Kotiveera Chari and A. Chennakesava Reddy, Numerical Simulation of Particulate Fracture in Round Silicon Nitride Particulate/AA6061 Alloy Metal Matrix Composites, National Conference on Materials and Manufacturing Processes, Hyderabad, India, 27-28 February 1998, pp. 110-114.
5. H. B. Niranjan and A. Chennakesava Reddy, Effect of Elastic Moduli Mismatch on Particulate Fracture in AA7020/Silicon Nitride Particulate Metal Matrix Composites , National Conference on Materials and Manufacturing Processes, Hyderabad, India, 27-28 February, 115-118, 1998

6. P. Martin Jebaraj and A. Chennakesava Reddy, Cohesive Zone Modelling for Interface Debonding in AA8090/Silicon Nitride Nanoparticulate Metal Matrix Composites, National Conference on Materials and Manufacturing Processes, Hyderabad, India, 27-28 February 1998, pp. 119-122.
7. P. Martin Jebaraj and A. Chennakesava Reddy, Plane Strain Finite Element Modeling for Interface Debonding in AA1100/Silicon Oxide Nanoparticulate Metal Matrix Composites, National Conference on Materials and Manufacturing Processes, Hyderabad, India, 27-28 February 1998, pp. 123-126.
8. A. Chennakesava Reddy, Local Stress Differential for Particulate Fracture in AA2024/Titanium Carbide Nanoparticulate Metal Matrix Composites, National Conference on Materials and Manufacturing Processes, Hyderabad, India, 27-28 February 1998, pp. 127-131.
9. B. Kotiveera Chari and A. Chennakesava Reddy, Interface Debonding and Particulate Facture based on Strain Energy Density in AA3003/MgO Nanoparticulate Metal Matrix Composites, National Conference on Materials and Manufacturing Processes, Hyderabad, India, 27-28 February 1998, pp. 132-136.
10. H. B. Niranjan and A. Chennakesava Reddy, Numerical and Analytical Prediction of Interface Debonding in AA4015/Boron Nitride Nanoparticulate Metal Matrix Composites , National Conference on Materials and Manufacturing Processes, Hyderabad, India, 27-28 February 1998, pp. 137-140.
11. S. Sundara Rajan and A. Chennakesava Reddy, Effect of Particulate Volume Fraction on Particulate Cracking in AA5050/Zirconium Oxide Nanoparticulate Metal Matrix Composites , National Conference on Materials and Manufacturing Processes, Hyderabad, India, 27-28 February 1998, pp. 156-159.
12. S. Sundara Rajan and A. Chennakesava Reddy, Cohesive Zone Analysis for Interface Debonding in AA6061/Titanium Nitride Nanoparticulate Metal Matrix Composites , National Conference on Materials and Manufacturing Processes, Hyderabad, India, 27-28 February 1998, pp. 160-164.
13. A. Chennakesava Reddy, Effect of Particle Loading on Microealstic Behavior and interfacial Tractions of Boron Carbide/AA4015 Alloy Metal Matrix Composites, 1st International Conference on Composite Materials and Characterization, Bangalore, 14-15 march 1997, pp. 176-179.7
14. A. Chennakesava Reddy, Reckoning of Micro-stresses and interfacial Tractions in Titanium Boride/AA2024 Alloy Metal Matrix Composites, 1st International Conference on Composite Materials and Characterization, Bangalore, 14-15 march 1997, pp. 195-197.
15. A. Chennakesava Reddy, Interfacial Debonding Analysis in Terms of Interfacial Tractions for Titanium Boride/AA3003 Alloy Metal Matrix Composites, 1st National Conference on Modern Materials and Manufacturing , Pune, India, 19-20 December 1997, pp. 124-127.
16. A. Chennakesava Reddy, Evaluation of Debonding and Dislocation Occurrences in Rhombus Silicon Nitride Particulate/AA4015 Alloy Metal Matrix Composites, 1st National Conference on Modern Materials and Manufacturing , Pune, India, 19-20 December 1997, pp. 278-282.